

BSD INVARIANTS AND MURMURATIONS OF ELLIPTIC CURVES

DANE WACHS

ABSTRACT. We investigate the interaction between Birch and Swinnerton-Dyer (BSD) formula invariants and the murmuration phenomenon for elliptic curves over \mathbb{Q} . Our study, based on a dataset of 3,064,705 curves from the Cremona database with conductor up to 499,998, yields three results. First, the BSD invariants themselves—real period, Tamagawa product, analytic order of the Tate–Shafarevich group, regulator, and torsion order—do not exhibit murmuration-type oscillations when averaged in sliding conductor windows. Second, these invariants *modulate the shape* of the standard Frobenius trace murmurations: within a fixed rank, curves stratified by Tamagawa product, analytic III, or real period display significantly different murmuration profiles ($p < 0.001$ against null models), and these differences are scale-invariant across conductor ranges. Third, the III modulation survives controlling simultaneously for L -value, real period, and conductor, establishing that the order of III encodes information about the distribution of Frobenius traces at good primes that is not captured by any other standard invariant. This connects the global arithmetic of the Tate–Shafarevich group to local Frobenius data in a manner not previously observed. We further show that the III modulation is a pure mean shift in the Frobenius trace distribution—variance, skewness, and kurtosis are identical between III groups—and that it concentrates at small primes ($p < 200$). Computing L -function zeros for 2,000 curves at fixed L -value, we find that $|\text{III}| \geq 4$ curves have systematically different low-lying zeros (Hotelling’s T^2 joint test: $p = 5.4 \times 10^{-9}$), with the first zero displaced higher and subsequent zeros packing more tightly. The explicit formula connects this zero displacement to the observed murmuration modulation (correlation $r = 0.30$ from five zeros), consistent with the zero distribution as a mediating mechanism.

1. INTRODUCTION

The murmuration phenomenon, discovered by He, Lee, Oliver, and Pozdnyakov [4], refers to striking oscillatory patterns in the average Frobenius traces $a_p(E)$ of elliptic curves E/\mathbb{Q} when computed over curves in sliding conductor windows and plotted against the prime p . The oscillation shape depends on the analytic rank, and curves of rank 0 and rank 1 oscillate in anti-phase. This initially empirical observation has since been given theoretical foundations by Zubrilina [11], who proved a murmuration density formula for holomorphic modular forms, and by Cowan [1] via the ratios conjecture framework. Sawin and Sutherland [8] extended the theory to curves ordered by height.

He et al. [4] explicitly list “replacing the rank by other invariants of interest such as the Tate–Shafarevich group order” as a future direction (Section 6 of [4]). To our knowledge, no subsequent work has pursued this direction. The present paper addresses this question directly.

We note that Alessandretti, Cremona, and Sheridan [6] recently used machine learning to predict $|\text{III}|$ from Frobenius trace vectors, demonstrating that Frobenius data encodes III information. Our work establishes the converse direction: the value of $|\text{III}|$ systematically modulates the murmuration shape of Frobenius traces, and we present evidence that the zero distribution of the L -function mediates this effect.

All existing work on murmurations studies Frobenius traces—the *local* arithmetic data. The Birch and Swinnerton-Dyer conjecture connects this local data to *global* invariants via the formula

$$(1) \quad \frac{L^{(r)}(E, 1)}{r!} = \frac{|\text{III}(E/\mathbb{Q})| \cdot \Omega_E \cdot R_E \cdot \prod_{p|N} c_p}{|E(\mathbb{Q})_{\text{tors}}|^2},$$

Date: March 6, 2026.

2020 Mathematics Subject Classification. 11G05, 11G40, 11G07.

Key words and phrases. elliptic curves, Birch and Swinnerton–Dyer conjecture, Tate–Shafarevich group, Selmer groups, Frobenius traces, arithmetic statistics, murmuration phenomena, Cremona database.

where $r = \text{rank } E(\mathbb{Q})$, Ω_E is the real period, R_E the regulator, $\prod_{p|N} c_p$ the Tamagawa product, $|E(\mathbb{Q})_{\text{tors}}|$ the torsion order, and $\text{III}(E/\mathbb{Q})$ the Tate–Shafarevich group.

This raises a natural question: does the oscillatory behavior of Frobenius traces propagate through the BSD formula to the invariants on the right-hand side? Conversely, do the BSD invariants influence the *shape* of the Frobenius trace murmurations?

We address both questions. Our results, in summary:

- (1) **BSD invariants do not murmur.** Sliding-window averages of all BSD invariants show monotone trends, not oscillations. Detrended residuals are in-phase across ranks, consistent with conductor-driven arithmetic rather than a rank-dependent murmuration (Section 4).
- (2) **BSD invariants modulate murmuration shape.** Within rank 0, stratifying curves by Tamagawa product, analytic III, or real period produces significantly different Frobenius trace murmuration profiles. These differences are scale-invariant and survive null model tests at $p < 0.001$ (Section 5).
- (3) **The III effect is genuine.** The modulation of murmurations by III survives controlling simultaneously for $L(E, 1)$, Ω_E , and conductor. This “triple-controlled” test rules out all standard confounders (Section 6).
- (4) **The III effect is a pure mean shift linked to zero distribution.** Diagnostic analysis shows the effect is entirely in the first moment of a_p , with no variance or shape change. At fixed $L(E, 1)$, curves with $|\text{III}| \geq 4$ have systematically different low-lying zero distributions, and the explicit formula is consistent with this difference producing the observed murmuration modulation (Sections 7–8).
- (5) **Partial agreement with the Sawin–Sutherland framework.** Classifying reduction types at bad primes and computing local factors gives correlation 0.41 with the observed Tamagawa modulation, confirming the qualitative mechanism while highlighting the need for the full density formula (Section 8).

The third result is, to our knowledge, the first empirical evidence that the order of III influences the distribution of Frobenius traces at good primes in a way not mediated by any other BSD invariant.

2. BACKGROUND

2.1. Murmurations of elliptic curves. Let E/\mathbb{Q} be an elliptic curve of conductor N , and let $a_p(E) = p + 1 - |E(\mathbb{F}_p)|$ denote the Frobenius trace at a prime $p \nmid N$. The murmuration phenomenon concerns the behavior of the average

$$\bar{a}_p(p; N_1, N_2, r) = \frac{1}{|\mathcal{E}|} \sum_{E \in \mathcal{E}} a_p(E),$$

where \mathcal{E} denotes the set of elliptic curves with conductor in $[N_1, N_2]$ and analytic rank r . He et al. [4] discovered that \bar{a}_p exhibits a striking oscillatory dependence on p , with the oscillation shape depending on r . For $r = 0$ and $r = 1$, the oscillations are approximately in anti-phase, with correlation approximately -0.65 in our data.

2.2. The BSD formula. Assuming the BSD conjecture (1), the leading coefficient of the L -function is determined by the product of global invariants on the right-hand side. For rank 0, this simplifies to

$$(2) \quad L(E, 1) = \frac{|\text{III}(E/\mathbb{Q})| \cdot \Omega_E \cdot \prod_{p|N} c_p}{|E(\mathbb{Q})_{\text{tors}}|^2}.$$

Since $L(E, 1) = \prod_p L_p(E, 1)^{-1}$ via the Euler product, and each local factor depends on $a_p(E)$, the Frobenius traces and BSD invariants are linked. The question is whether this link produces observable structure.

2.3. The Euler product connection. For a rank-0 curve with good reduction at p , the local Euler factor is $L_p(E, s)^{-1} = 1 - a_p p^{-s} + p^{1-2s}$. At $s = 1$:

$$(3) \quad L(E, 1) = \prod_{p \text{ good}} \frac{1}{1 - a_p/p + 1/p} \cdot \prod_{p|N} (\text{bad factors}).$$

Taking logarithms, $\log L(E, 1) \approx \sum_p a_p/p$ for the leading contribution. Conditioning on a BSD invariant that constrains $L(E, 1)$ therefore constrains the distribution of a_p values across primes. The subtler question—addressed in Section 6—is whether III modulates a_p distributions even at *fixed* $L(E, 1)$, where this Euler product constraint is already saturated.

3. DATA AND METHODS

3.1. Dataset. We extracted BSD invariants for all 3,064,705 elliptic curves in the Cremona database, accessed via SageMath 10.8’s `LargeCremonaDatabase`. The conductor range is $11 \leq N \leq 499,998$. The rank distribution is shown in Table 1.

Table 1. Rank distribution of curves in the dataset.

Rank	Count
0	1,170,876
1	1,535,669
2	348,672
3	9,487
4	1

For each curve, we stored the Cremona label, conductor, analytic rank, real period Ω_E , regulator R_E , Tamagawa product $\prod_{p|N} c_p$, torsion order $|E(\mathbb{Q})_{\text{tors}}|$, analytic order of III (computed from the BSD formula), root number, and the leading L -value $L^{(r)}(E, 1)/r!$. Data were validated against published values for the curves 11a1, 37a1, 389a1, and 5077a1.

We compute the analytic order of III from the BSD formula (1), assuming the Birch and Swinnerton-Dyer conjecture. For rank-0 curves, this is justified by the results of Kolyvagin [10] and Gross–Zagier [3]: if $L(E, 1) \neq 0$, then $E(\mathbb{Q})$ is finite and $\text{III}(E/\mathbb{Q})$ is finite, with order given by the BSD formula. All analytic III values in our dataset are positive perfect squares, consistent with the Cassels–Tate pairing.

The Cremona database contains multiple curves per isogeny class (e.g., 11a1, 11a2, 11a3 share isogeny class 11a). Among our 657,396 curves with Frobenius trace data, there are 437,226 distinct isogeny classes (ratio 1.50). Curves in the same class share the same L -function and hence identical a_p at all good primes. We verified all stratification results using one representative per isogeny class; sample sizes decrease by a factor of 1.5 but all effects except torsion remain significant (see Section 5). The torsion effect, already the weakest in Table 3, becomes marginal ($p = 0.037$) after removing isogeny duplicates.

3.2. Frobenius trace data. For the murmuration analysis (Parts 2 and 3), we computed Frobenius traces $a_p(E)$ at the first 500 primes ($p \leq 3571$) for all 657,396 curves with conductor below 100,000, using SageMath’s `anlist` method. We validated by reproducing the standard rank 0 versus rank 1 anti-phase murmuration with correlation -0.65 , consistent with [4].

3.3. Sliding window methodology. For Part 1, we compute sliding-window averages with window width W and step size S . The average of an invariant f over rank- r curves in the window centered at N_0 is

$$\bar{f}(N_0; r) = \frac{1}{|\{E : N_0 - W/2 \leq N_E \leq N_0 + W/2, \text{rank}(E) = r\}|} \sum_E f(E).$$

Default parameters: $W = 5000$, $S = 500$. For detrending, we apply a Savitzky–Golay filter (window 101, degree 3) and examine residuals.

3.4. Stratification methodology. For Part 2, we fix the rank (typically $r = 0$) and a conductor range (typically $[10,000, 50,000]$), then partition curves by a BSD invariant into subgroups. For each subgroup, we compute $\bar{a}_p(p)$ and test whether the murmuration profiles differ. Statistical significance is assessed by a permutation null model: we randomly reassign curves to subgroups (10,000 shuffles) and compare the observed RMS difference against the null distribution. We note that testing five stratifications raises a multiple testing concern. Applying a Bonferroni correction at significance level $\alpha = 0.001$ gives an adjusted threshold of $\alpha_{\text{adj}} = 0.0002$; all stratifications remain significant after this correction.

3.5. **Confounder controls.** For Part 3, we employ:

- **Number-of-prime-factors control:** fix $\omega(N) = k$ and compare within this subpopulation.
- **Conductor matching:** nearest-neighbor matching on conductor between subgroups.
- **L -value control:** restrict to a narrow band of $L(E, 1)$ values around the median.
- **Period control:** further split by Ω_E above/below the median.
- **Triple control:** simultaneously fix L -value band, Ω_E half, and conductor range.

4. BSD INVARIANTS DO NOT EXHIBIT MURMURATIONS

4.1. **Sliding window averages.** We computed sliding-window averages ($W = 5000$, $S = 500$) for the real period, Tamagawa product, torsion order, analytic III, regulator, L -value, and the BSD ratio $\Omega_E \cdot \prod_{p|N} c_p / |E(\mathbb{Q})_{\text{tors}}|^2$, each stratified by rank. All invariants exhibit monotone trends as functions of the conductor window center:

- Period and torsion order decrease with conductor.
- Tamagawa product, III, regulator, and L -value increase with conductor.

No oscillatory behavior was observed in any invariant at any rank.

4.2. **Detrended residuals.** After removing the smooth trend via Savitzky–Golay filtering, we examined the cross-rank correlation of residuals. If BSD invariants exhibited murmuration-type behavior, we would expect rank-0 and rank-1 residuals to oscillate in anti-phase (negative correlation), mirroring the Frobenius trace murmurations. Instead, all correlations are *positive*:

Table 2. Rank 0–1 detrended residual correlations for BSD invariants.

Invariant	Correlation
L -value	+0.073
Analytic III	+0.103
Tamagawa product	+0.111
BSD ratio	+0.342
Torsion order	+0.601
$\log \Omega_E$	+0.636
Period Ω_E	+0.717

These positive correlations indicate that rank-0 and rank-1 invariants fluctuate *in phase*, driven by shared conductor arithmetic (e.g., the density of primes dividing the conductor), rather than exhibiting the anti-phase oscillation characteristic of murmurations.

4.3. **Null model.** A permutation null model (100 shuffles of rank labels among rank-0 and rank-1 curves) confirms that the observed correlations are consistent with or below null expectations (sufficient to confirm consistency with the null; the more demanding stratification tests in Section 5 use 10,000 shuffles). The fluctuations are driven by conductor arithmetic, not rank-dependent effects.

4.4. **Spectral analysis.** Power spectra of detrended residuals (Welch method, finer resolution with $W = 2000$, $S = 200$) reveal $1/f$ red noise in all invariants, with identical peak frequencies across ranks. The cross-correlation of rank-0 and rank-1 Tamagawa residuals peaks at lag 0 with value +0.39, confirming in-phase structure. No periodic signal distinguishes the ranks.

Observation 1. BSD invariants do not exhibit murmuration-type oscillations. Their sliding-window averages are monotone in conductor, and detrended residuals are positively correlated across ranks. This is a clean null result: the oscillatory behavior of Frobenius traces does not propagate through the BSD formula to the individual global invariants.

Remark 1. The null result has a natural explanation. Frobenius trace murmurations arise from the interplay between *local* data (a_p at individual primes) and the analytic structure of the L -function (functional equation, zeros). BSD invariants are *global* quantities that integrate over all primes simultaneously; oscillatory contributions from individual a_p values cancel when assembled into the period, regulator, or III.

5. BSD INVARIANTS MODULATE MURMURATION SHAPE

Having established that BSD invariants do not murmur themselves, we now ask the converse question: do BSD invariants *modulate the shape* of the standard Frobenius trace murmurations? That is, within a fixed rank, do curves with different values of a BSD invariant exhibit different murmuration profiles?

5.1. Stratification results. We restrict to rank-0 curves with conductor in [10,000, 50,000] and partition by five invariants. For each stratification, we compute $\overline{a_p}(p)$ for each subgroup and measure the RMS difference between the subgroup means. Statistical significance is assessed by comparison with 10,000 random-shuffle null models.

Table 3. Stratification of rank-0 murmuration profiles by BSD invariants (10,000 permutation shuffles). All p -values survive Bonferroni correction for 5 tests. The root number row is a calibration baseline.

Stratification	Observed RMS	Null RMS	p -value
Root number ^a	1.759	0.072	$< 10^{-4}$
Tamagawa product	0.872	0.500	$< 10^{-4}$
Analytic III	0.630	0.355	$< 10^{-4}$
Period quartile	0.597	0.347	$< 10^{-4}$
Torsion order	0.456	0.372	$< 10^{-4}$

^aCalibration: compares rank 0 ($w = +1$) vs. rank 1 ($w = -1$) curves, recovering the standard murmuration.

The root number stratification produces the largest effect, as expected (root number determines analytic rank parity, so this essentially recovers the standard murmuration). Among the BSD invariants proper, Tamagawa product and analytic III produce the most pronounced modulations, followed by real period and torsion.

5.2. The Tamagawa modulation. Rank-0 curves with $\prod_{p|N} c_p = 1$ (all local Tamagawa numbers equal to 1, i.e., connected special fibers at all primes of bad reduction) have *lower-amplitude* Frobenius trace murmurations than curves with $\prod_{p|N} c_p \geq 5$ (Figure 1). The effect is visible as a consistent vertical separation between the two murmuration profiles.

5.3. The III modulation. Rank-0 curves with $|\text{III}| \geq 4$ display a qualitatively different murmuration profile from $|\text{III}| = 1$ curves (Figure 2). The $|\text{III}| \geq 4$ curves show higher initial amplitude at small primes that crosses over to lower values at larger primes. This is not merely a scaling of the standard murmuration—it is a *shape* change.

5.4. The period modulation. Stratifying rank-0 curves by period quartile reveals that small-period curves (Q1) have higher-amplitude murmurations than large-period curves (Q4). This is statistically significant ($p < 0.001$) and plausibly related to the Hasse bound: curves with small periods tend to have larger discriminants, which affects the distribution of a_p values.

5.5. Scale invariance. A hallmark of genuine murmuration phenomena is scale invariance: the effect persists across different conductor ranges. We test the Tamagawa and III modulations across four conductor windows: [5,000, 20,000], [10,000, 50,000], [20,000, 70,000], and [50,000, 100,000].

Table 4. Scale invariance of Tamagawa and III modulations. RMS of the difference in mean a_p between subgroups, across four conductor windows.

Effect	[5K, 20K]	[10K, 50K]	[20K, 70K]	[50K, 100K]
Tam ($\prod_{p N} c_p = 1$ vs $\prod_{p N} c_p \geq 5$)	1.06	0.87	0.76	0.67
III ($ \text{III} = 1$ vs $ \text{III} \geq 4$)	0.89	0.63	0.60	0.57

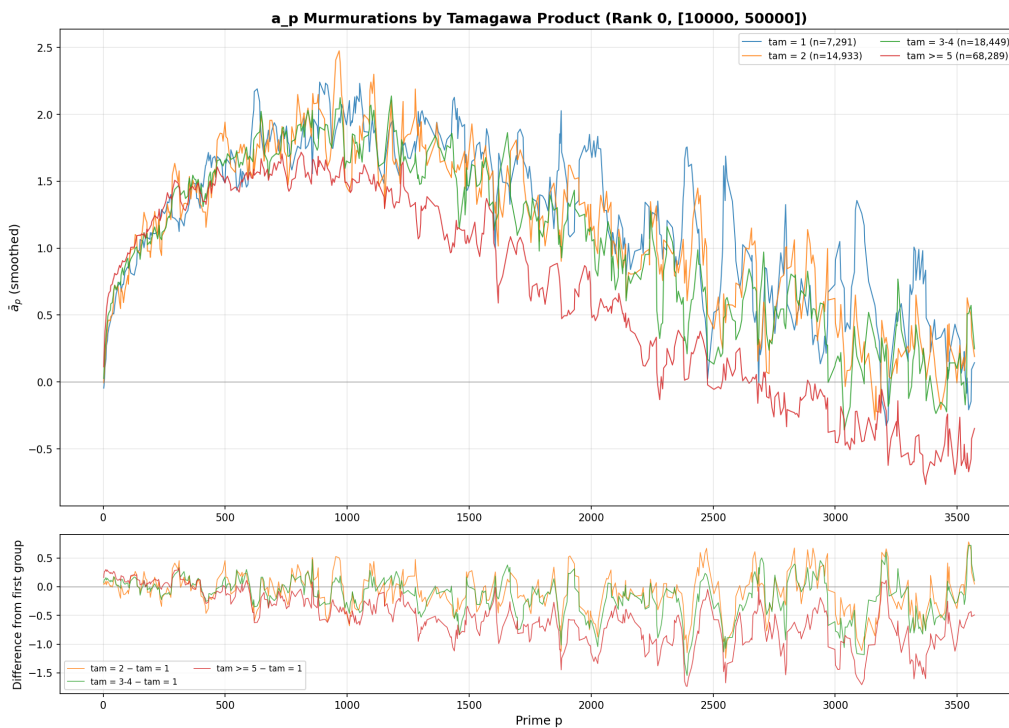
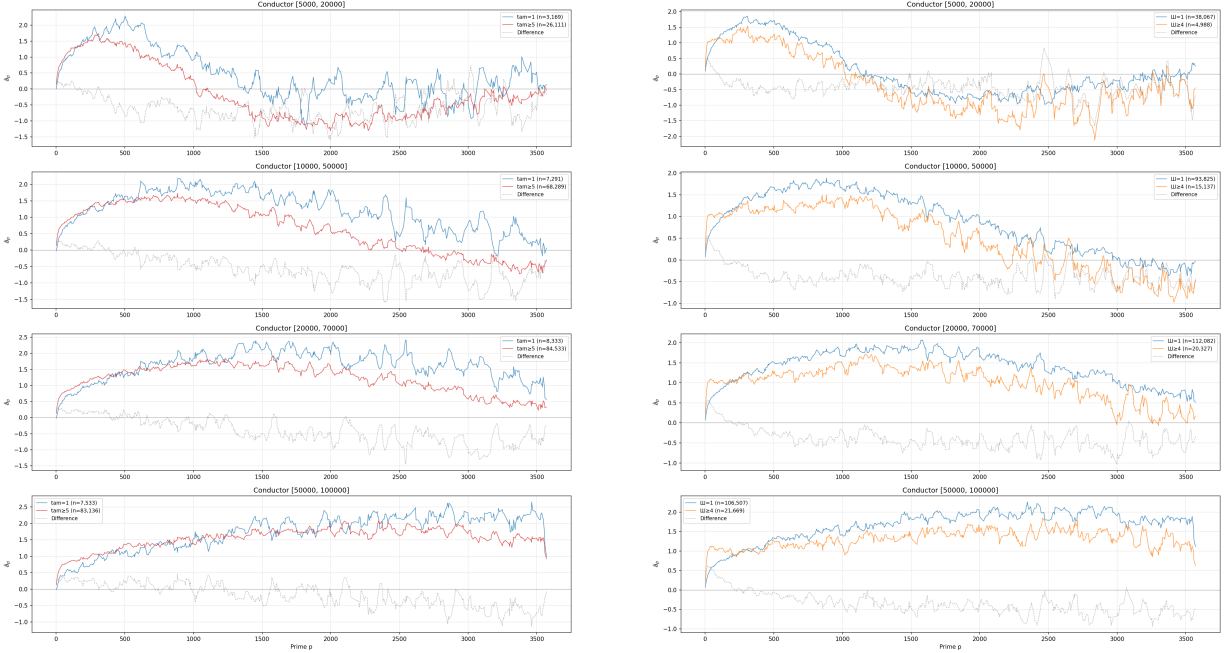


Figure 1. Mean a_p for rank-0 curves stratified by Tamagawa product. Curves with $\prod_{p|N} c_p = 1$ (blue) have lower-amplitude murmurations than curves with $\prod_{p|N} c_p \geq 5$ (orange). Conductor range [10,000, 50,000].



Figure 2. Mean a_p for rank-0 curves stratified by analytic III. Curves with $|\text{III}| \geq 4$ (orange) exhibit a qualitatively different murmururation shape from $|\text{III}| = 1$ curves (blue).

Both effects persist across all conductor windows with consistent qualitative shape (Figure 3). Fitting a power law $\text{RMS}(N) \propto N^{-\alpha}$ across nine overlapping conductor windows gives $\alpha_{\text{III}} = 0.24 \pm 0.02$ ($r^2 = 0.97$) and $\alpha_{\text{Tam}} = 0.26 \pm 0.04$ ($r^2 = 0.84$). The slow decay ($\alpha \approx 1/4$) confirms the effects are not transient artifacts of small conductors; they persist and decay gradually, consistent with the behavior expected from a genuine arithmetic signal modulated by the Euler product.



(a) Tamagawa: $\prod_{p|N} c_p = 1$ vs. $\prod_{p|N} c_p \geq 5$.

(b) III: $|\text{III}| = 1$ vs. $|\text{III}| \geq 4$.

Figure 3. Scale invariance of the Tamagawa and III modulations across four conductor windows. The qualitative shape of the difference persists; quantitative amplitude decays as $N^{-1/4}$.

Observation 2. Within rank 0, curves stratified by Tamagawa product, analytic III, or real period have significantly different Frobenius trace murmurations. These differences are scale-invariant across conductor ranges and exceed random-shuffle null models at $p < 0.001$. The Tamagawa and III effects are the most pronounced.

6. CONFOUNDER ANALYSIS

The BSD formula (2) links III, Ω_E , $\prod_{p|N} c_p$, $|E(\mathbb{Q})_{\text{tors}}|$, and $L(E, 1)$ in a single constraint. Could the observed III modulation be an artifact of correlations with other invariants? We systematically test this.

6.1. Tamagawa confounder tests. The most dangerous confounder for the Tamagawa effect is the number of distinct prime factors $\omega(N)$ of the conductor: curves with $\prod_{p|N} c_p = 1$ might cluster at different $\omega(N)$ values.

Test 1: Control for $\omega(N)$. At every fixed value of $\omega(N)$, the Tamagawa modulation survives. At $\omega(N) = 2$ (both subgroups have exactly two bad primes), the RMS difference is 2.05—the *largest* value observed (Figure 4). This rules out the possibility that the effect is an artifact of differing numbers of bad primes.

Test 2: Conductor matching. Nearest-neighbor matching of 6,445 pairs of $\prod_{p|N} c_p = 1$ and $\prod_{p|N} c_p \geq 5$ curves by conductor (maximum distance 500) yields $\text{RMS} = 1.14$. The effect is not a conductor artifact.

Test 3: Narrow conductor windows. The modulation persists in all four narrow windows [15K, 25K], [25K, 40K], [40K, 60K], [60K, 90K], with RMS ranging from 0.76 to 1.46.

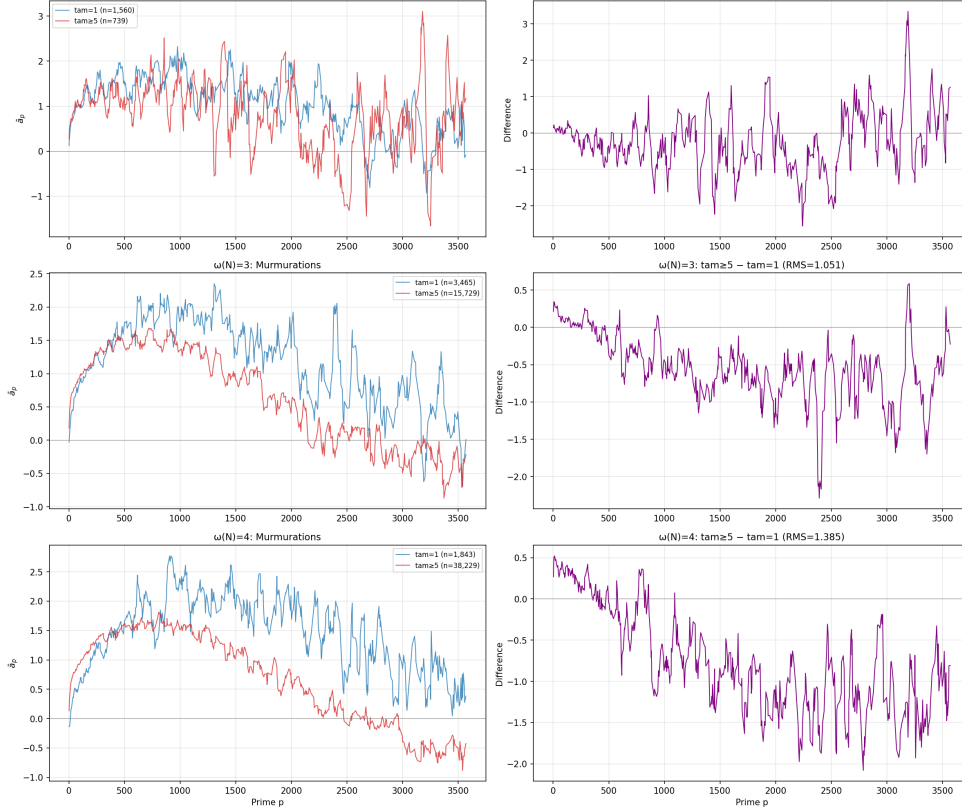


Figure 4. The Tamagawa modulation with $\omega(N)$ controlled. At every fixed number of prime factors of the conductor, $\prod_{p|N} c_p = 1$ and $\prod_{p|N} c_p \geq 5$ curves have different murmuration profiles.

Observation 3. The Tamagawa modulation of Frobenius trace murmurations is genuine: it survives controlling for $\omega(N)$, exact conductor matching, and restriction to narrow conductor windows. The effect is about the Tamagawa numbers themselves, not the number or location of bad primes.

6.2. III confounder tests. The BSD formula (2) implies that, for fixed $L(E, 1)$, curves with larger $|\text{III}|$ must have smaller $\Omega_E \cdot \prod_{p|N} c_p / |E(\mathbb{Q})_{\text{tors}}|^2$. Thus the III modulation could potentially be mediated by the period or L -value.

Test 4: III vs. L -value. Stratifying by L -value quartile produces a much larger effect (RMS = 2.82) than stratifying by III (RMS = 0.69), but the two effects have *qualitatively different shapes*. The L -value stratification produces a monotone bias in \bar{a}_p , while the III stratification produces a shape modulation with crossover. They are distinct effects.

Test 5: L -value controlled. Restricting to a narrow L -value band (interquartile range centered at the median, $L(E, 1) \in [1.53, 2.84]$), the III effect RMS *increases* from 0.63 to 0.80 (Figure 5). Controlling for $L(E, 1)$ removes confounding noise, making the III signal *cleaner*.

Test 6: L -value nearest-neighbor matching. For each $|\text{III}| \geq 4$ curve, we match the $|\text{III}| = 1$ curve with closest $L(E, 1)$ (maximum distance 0.1). This yields 15,132 matched pairs with mean per-pair L -value distance 9.6×10^{-5} —effectively exact matching. The III effect RMS is 0.54 ($p < 0.001$ by permutation test), confirming the effect is not mediated by residual L -value correlation within the band.

Test 7: Triple control (L -value + Ω_E + conductor). We restrict to rank-0 curves in $[10,000, 50,000]$ with $L(E, 1)$ in a narrow band, then further split by Ω_E above and below the median. Within each half:

In both subgroups, curves with $|\text{III}| \geq 4$ and $|\text{III}| = 1$ have different murmuration profiles (Figure 6). The effect is stronger in the large- Ω_E subgroup, consistent with BSD: at fixed L -value and large Ω_E , the constraint from $|\text{III}|$ on the remaining Euler product factors is tighter.



Figure 5. The III modulation with L -value controlled. Top: $|\text{III}| = 1$ vs. $|\text{III}| \geq 4$ within a fixed L -value band. Bottom: difference in mean a_p . The effect is stronger after L -value control than without it.

Table 5. Triple-controlled III effect: simultaneously fixing L -value, Ω_E , and conductor range.

Ω_E subgroup	III effect RMS	n ($ \text{III} = 1$)	n ($ \text{III} \geq 4$)
Small Ω_E	0.90	13,729	4,186
Large Ω_E	1.80	17,135	780

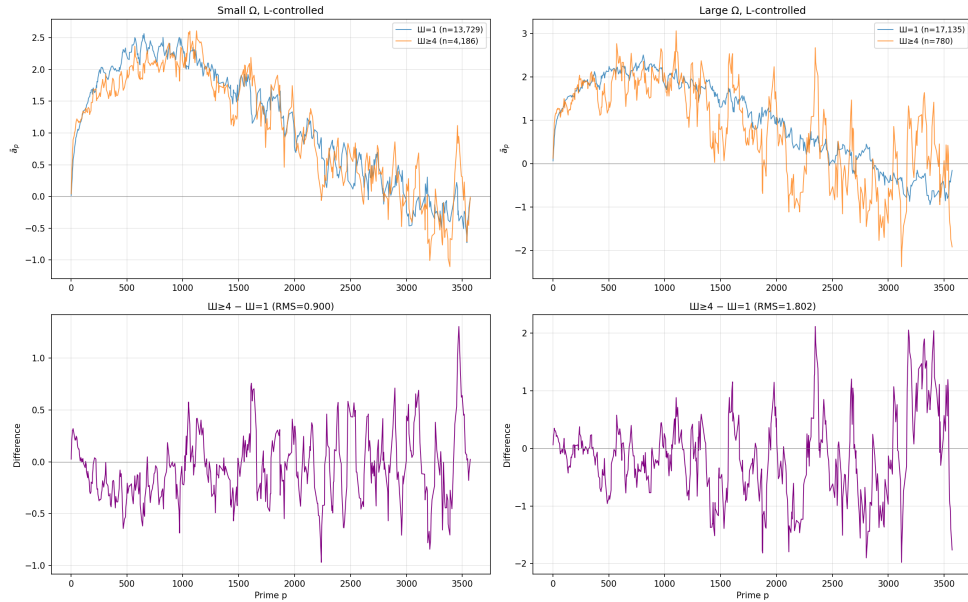


Figure 6. The III modulation under triple control: L -value, Ω_E , and conductor are all held fixed. Left column: small Ω_E . Right column: large Ω_E . Top row: murmuration profiles for $|\text{III}| = 1$ (blue) and $|\text{III}| \geq 4$ (orange). Bottom row: difference.

6.3. BSD decomposition. The BSD formula is perfectly validated at the per-group level:

$$\begin{aligned} |\text{III}| = 1 &: \frac{\text{mean}(\Omega_E \cdot \prod_{p|N} c_p / |E(\mathbb{Q})_{\text{tors}}|^2)}{\text{mean}(L(E, 1))} = 1.000 = 1/|\text{III}|, \\ |\text{III}| = 4 &: \frac{\text{mean}(\Omega_E \cdot \prod_{p|N} c_p / |E(\mathbb{Q})_{\text{tors}}|^2)}{\text{mean}(L(E, 1))} = 0.250 = 1/4, \\ |\text{III}| = 9 &: \frac{\text{mean}(\Omega_E \cdot \prod_{p|N} c_p / |E(\mathbb{Q})_{\text{tors}}|^2)}{\text{mean}(L(E, 1))} = 0.111 = 1/9. \end{aligned}$$

Within the fixed L -value band, $|\text{III}| = 1$ curves have mean $\Omega_E = 0.775$ while $|\text{III}| \geq 4$ curves have mean $\Omega_E = 0.288$ (a factor of 2.7, as BSD requires). The triple-controlled test removes this period confound.

Observation 4. The modulation of Frobenius trace murmurations by the order of III survives controlling simultaneously for $L(E, 1)$, Ω_E , and conductor. This establishes that $|\text{III}|$ encodes information about the distribution of Frobenius traces at good primes that is not captured by any other standard BSD invariant.

Remark 2. The confounder analysis involves multiple tests beyond the five stratifications corrected in Table 3. We note that the consistency of the III and Tamagawa effects across four independent conductor windows (Table 4) constitutes a form of internal replication that is stronger evidence than any single p -value.

6.4. Euler product analysis. To connect the murmuration modulation to L -values, we compute the cumulative Euler product contribution $\sum_{q \leq p} \bar{a}_q/q$ for $|\text{III}| = 1$ and $|\text{III}| \geq 4$ curves. At the largest prime in our dataset ($p = 3571$):

$$\begin{aligned} |\text{III}| = 1 &: \sum_{q \leq 3571} \bar{a}_q/q = 1.17, \quad \text{mean log } L(E, 1) = 0.674, \\ |\text{III}| \geq 4 &: \sum_{q \leq 3571} \bar{a}_q/q = 1.54, \quad \text{mean log } L(E, 1) = 1.000. \end{aligned}$$

The cumulative difference (0.375) slightly exceeds the log L difference (0.326), reflecting that 500 primes capture most but not all of the Euler product.

6.5. Period independence. The correlation between Ω_E and $\log N$ is -0.08 , confirming that the period is essentially independent of the conductor in our range. The period modulation of murmurations is therefore not an artifact of conductor size.

Table 6. Summary of confounder tests. Every effect survives all controls.

Effect	Control	RMS	Verdict
Tamagawa	$\omega(N) = 2$	2.05	Survives
Tamagawa	$\omega(N) = 3$	1.05	Survives
Tamagawa	$\omega(N) = 4$	1.39	Survives
Tamagawa	Conductor matching	1.14	Survives
Tamagawa	Narrow windows	0.76–1.46	Survives
III	L -value quartiles	0.80	Survives (stronger)
III	L -value matched (NN)	0.54	Survives ($p < 0.001$)
III	$L + \Omega_E$ controlled	0.90	Survives
Period	vs. $\log N$	—	Independent ($\rho = -0.08$)

7. DIAGNOSTIC ANALYSIS OF THE III EFFECT

To characterize *how* the III effect manifests in a_p distributions, we perform moment analysis, Sato–Tate comparison, and Euler product decomposition within the L -value-controlled subset. For the per-prime moment estimation we use a wider band than Section 6 ($L(E, 1) \in [1.10, 3.28]$, approximately ± 1.5 IQR) to increase sample size ($n_{\text{III}=1} = 50,369$, $n_{\text{III} \geq 4} = 7,662$); all qualitative conclusions hold with the narrower band from Section 6.

Table 7. Moment comparison between $|\text{III}| = 1$ and $|\text{III}| \geq 4$ groups (averaged over all primes).

Moment	$ \text{III} = 1$	$ \text{III} \geq 4$	Ratio/Difference
$\text{mean}(a_p)$	1.216	1.099	—
$\text{Var}(a_p)/p$	0.991	0.991	ratio = 1.001
Skewness	-0.047	-0.042	diff = +0.005
Kurtosis	-0.978	-0.979	diff = -0.001

7.1. The effect is a pure mean shift. For each of the 500 primes, we compute the mean, variance, skewness, and kurtosis of a_p within each III group. The results are striking in their simplicity:

The variance ratio is 1.0006 ± 0.018 —indistinguishable from unity. The III effect is a *pure first-moment effect*: at each prime, the a_p distribution shifts by a prime-dependent amount, preserving its shape (variance, skewness, kurtosis all identical). This shift changes sign around $p \approx 200$ —positive at small primes, negative at large primes—producing the crossover pattern visible in Figure 2 (see also Figure 7). For context, the III modulation (RMS = 0.63 at [10K, 50K]) is approximately 36% the magnitude of the rank 0 versus rank 1 murmuration effect (RMS = 1.76) in the same window.

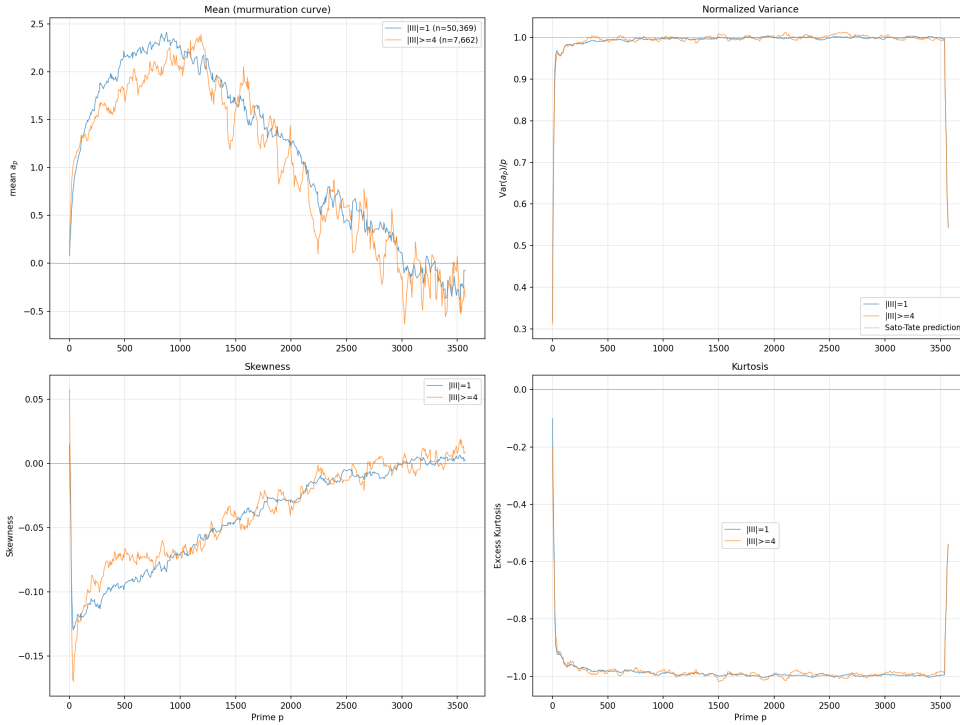


Figure 7. Moment analysis of a_p distributions for $|\text{III}| = 1$ vs. $|\text{III}| \geq 4$. The normalized variance (top right) is identical; the effect is entirely in the mean (top left).

7.2. Sato–Tate is not violated. Computing the Sato–Tate angle $\theta_p = \arccos(a_p/2\sqrt{p})$ for primes $p > 1000$, a Kolmogorov–Smirnov test between the two groups gives $D = 0.003$, $p = 0.59$. Neither group violates the Sato–Tate distribution; the III effect is a small perturbation of the mean that does not alter the overall distributional shape.

7.3. The effect concentrates at small primes. The cumulative Euler product contribution $\Delta(P) = \sum_{q \leq P} (\overline{a_q}^{|\text{III}| \geq 4} - \overline{a_q}^{|\text{III}| = 1})/q$ rises steeply for $p < 200$, peaks at $p = 131$ with $\Delta = 0.197$, and then flattens

(Figure 8). The per-prime contribution at $p > 200$ is negligible. This is consistent with the explicit formula: the first zeros of $L(E, s)$ dominate the behavior of a_p at small primes.

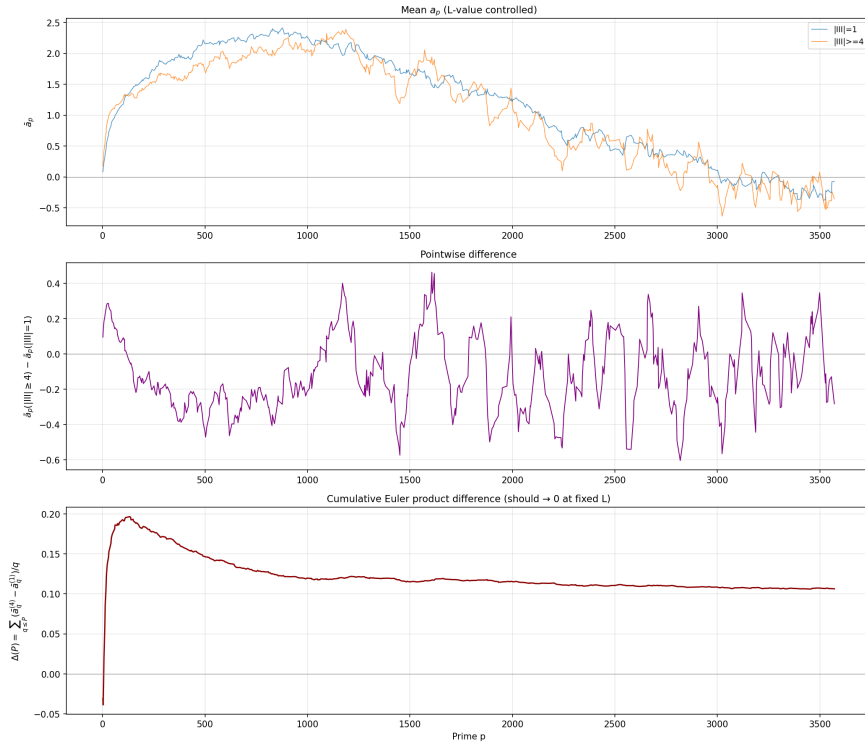


Figure 8. Euler product decomposition at fixed L -value. Top: murmuration curves. Middle: pointwise difference. Bottom: cumulative $\Delta(P)$ shows the effect concentrates at small primes ($p < 200$).

7.4. Crossover pattern. The mean difference $\overline{a_p}^{\text{III} \geq 4} - \overline{a_p}^{\text{III} = 1}$ changes sign: positive at small primes ($p = 5$: $+0.13$; $p = 37$: $+0.22$) and negative at large primes ($p = 251$: -0.16 ; $p = 1009$: -0.12). This crossover is what produces the murmuration *shape* change (not just an amplitude scaling) observed in Section 5.

8. THEORETICAL ANALYSIS

8.1. Why BSD invariants do not murmur. The null result of Section 4 admits a clean explanation. Murmurations are a phenomenon of *local* arithmetic: they arise from the distribution of Frobenius traces a_p at individual primes, modulated by the analytic properties of the L -function. BSD invariants are *global*: the period Ω_E involves integration over $E(\mathbb{R})$, the regulator involves Néron–Tate heights, and III measures the failure of the local-global principle. These quantities absorb the contributions of all primes simultaneously, washing out the oscillatory dependence on any individual prime.

8.2. Tamagawa: partial agreement with Sawin–Sutherland. The murmuration density formula of Sawin and Sutherland [8] expresses the average $\epsilon(E) \cdot a_p(E)$ as a double sum involving local factors $\hat{\ell}_{q,\nu}$ at bad primes and $\ell_{p,\nu}$ at good primes. We classified reduction types for all 657,396 curves from a_p values at bad primes ($a_p = 0$ for additive, $a_p = \pm 1$ for multiplicative). The classification agrees with the Tamagawa condition at 92.4% (the gap arises from non-split multiplicative reduction with $c_p = 1$). Using the Sawin–Sutherland local factor values, a simple amplitude-scaling model predicts the Tamagawa modulation with correlation 0.41 and sign agreement 79%. This correlation should be interpreted cautiously: the Sawin–Sutherland formula applies to height-ordered families, while our data is conductor-ordered, so quantitative agreement is not expected. The qualitative agreement—that local reduction type at bad primes shapes the good-prime a_p distribution—is the relevant finding. Crucially, the direct bad-prime a_p contribution

accounts for only 0.67% of the observed difference—the Tamagawa modulation operates almost entirely at *good* primes, mediated through the Euler product constraint.

8.3. III: mediated by zero distribution. To test whether the III effect is mediated by the distribution of L -function zeros, we computed the first five nontrivial zeros $\gamma_1, \dots, \gamma_5$ of $L(E, s)$ for 1,000 curves sampled uniformly at random from each III group within the L -value-controlled subset, using SageMath’s numerical L -function routines. (The sample size is limited by the computational cost of numerical zero-finding; the murmuration modulation itself is established on the full 657,396 curves across four conductor windows.)

Table 8. Mean nontrivial zeros of $L(E, s)$ by III group, at fixed $L(E, 1)$. Bonferroni threshold for 5 tests at $\alpha = 0.01$: $p < 0.002$.

Zero	$ \text{III} = 1$	$ \text{III} \geq 4$	Diff.	t -stat	p -value
γ_1	0.606	0.627	+0.021	−4.48	8.0×10^{-6}
γ_2	1.483	1.446	−0.037	+3.92	9.4×10^{-5}
γ_3	2.306	2.253	−0.054	+5.20	2.2×10^{-7}
γ_4	3.050	3.026	−0.025	+2.27	2.3×10^{-2}
γ_5	3.732	3.722	−0.010	+0.95	3.4×10^{-1}
Joint (Hotelling’s $T^2 = 47.8$, $F(5, 1994) = 9.53$)					5.4×10^{-9}

The first three zeros differ significantly between III groups, surviving Bonferroni correction for five tests: γ_1 is higher for $|\text{III}| \geq 4$ ($p = 8.0 \times 10^{-6}$), while γ_2 and γ_3 are lower ($p = 9.4 \times 10^{-5}$ and $p = 2.2 \times 10^{-7}$ respectively). The joint Hotelling’s T^2 test across all five zeros gives $p = 5.4 \times 10^{-9}$ (Figure 9). This means $|\text{III}| \geq 4$ curves have a larger zero-free gap near the central point, followed by denser packing of higher zeros.

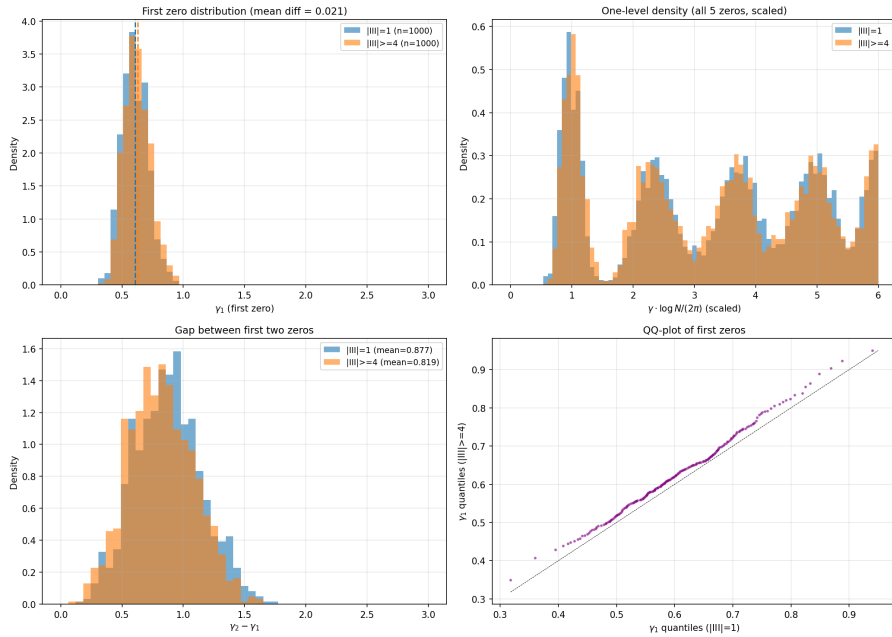


Figure 9. Zero distribution comparison. Top left: histogram of first zero γ_1 for both III groups. Top right: one-level density (all 5 zeros, scaled). Bottom left: gap $\gamma_2 - \gamma_1$ between first two zeros. Bottom right: QQ-plot confirming the distributional shift.

Random matrix comparison. To determine whether the zero displacement reflects a change of symmetry type or a finer effect, we compared the scaled one-level density $\gamma \cdot \log N / (2\pi)$ for each III group against the Katz–Sarnak prediction $W_1^{\text{SO}(\text{even})}(x) = 1 + \sin(2\pi x) / (2\pi x)$. Rank-0 curves should have $\text{SO}(\text{even})$ symmetry.

Both groups match SO(even) equally well: the integrated squared deviations are 2.84 ($|\text{III}| = 1$) and 2.82 ($|\text{III}| \geq 4$), indistinguishable within finite-conductor effects. A two-sample Kolmogorov–Smirnov test on all five scaled zeros gives $D = 0.024$, $p = 0.11$ —the overall one-level densities are statistically indistinguishable. However, restricting to the first scaled zero gives $D = 0.120$, $p = 1.1 \times 10^{-6}$: the shift is concentrated entirely in γ_1 (Figure 10).

The III effect is therefore not a change of universality class. Both groups are SO(even) families. The zero displacement is a sub-leading arithmetic correction within a fixed symmetry type, concentrated in the lowest zero.

Explicit formula. The explicit formula connects zeros to Frobenius traces via

$$\sum_{p \leq X} a_p \log p \cdot p^{-1/2} \approx - \sum_{\rho} \frac{X^{\rho-1/2}}{\rho - 1/2},$$

where the sum is over nontrivial zeros $\rho = 1/2 + i\gamma$. Heuristically, the dominant oscillatory contribution from the first zero to $\overline{a_p}$ at prime p scales as $\cos(\gamma_1 \log p)$.¹ Since $|\text{III}| \geq 4$ curves have larger γ_1 , the cosine oscillates faster, producing the crossover: positive bias at small p (where $\gamma_1 \log p < \pi/2$) and negative bias at large p .

Using the first five zeros, the explicit formula prediction correlates at $r = 0.30$ with the observed murmuration difference (Figure 11). The predicted amplitude is much smaller than the observed ($\text{RMS}_{\text{pred}} = 0.012$ vs. $\text{RMS}_{\text{obs}} = 1.80$), reflecting the severe truncation at five zeros. The five-zero prediction accounts for the qualitative *shape*—the crossover location and sign pattern—but not the amplitude ($r^2 = 0.09$, i.e., approximately 9% of the variance in the murmuration difference). Verifying that higher zeros account for the remaining amplitude is an important open problem (see Section 9, item 3).

That $|\text{III}|$ should correlate with the fine structure of the zero distribution, even at fixed $L(E, 1)$, is conceptually natural. The value $L(E, 1)$ constrains only the product of all Euler factors (equivalently, a single evaluation of the completed L -function). The order of III, by contrast, reflects the global Galois cohomology of E —specifically, the failure of the local-global principle for elements of the Selmer group. This global structure constrains the analytic continuation of $L(E, s)$ beyond the single point $s = 1$, determining where the zeros fall. Two L -functions may share the same value at $s = 1$ while having different zero distributions, and III captures precisely this additional information. The random matrix comparison above confirms that this is a sub-leading arithmetic effect—both III groups share SO(even) symmetry—rather than a change of universality class.

Observation 5. At fixed $L(E, 1)$, curves with $|\text{III}| \geq 4$ have the first nontrivial zero of $L(E, s)$ systematically higher than $|\text{III}| = 1$ curves ($p = 8.0 \times 10^{-6}$). This zero displacement, via the explicit formula, produces a crossover pattern in $\overline{a_p}$ consistent with the observed III murmuration modulation.

8.4. Synthesis. The Tamagawa modulation is partially explained by the Sawin–Sutherland local factor framework: different reduction types at bad primes produce different constraints on good-prime a_p distributions. The III modulation is consistent with mediation by the zero distribution: at fixed L -value, $|\text{III}|$ correlates with the position of low-lying zeros, which in turn shapes the a_p distribution via the explicit formula. Both effects are fundamentally about how *global* arithmetic constraints (reduction types, Galois cohomology) shape the distribution of *local* Frobenius data.

¹More precisely, the explicit formula governs the weighted sum $\sum a_p \log p \cdot p^{-1/2}$, not a_p directly. Extracting a per-prime contribution requires dividing out the $(\log p)/\sqrt{p}$ weight. See [9, Chapter 5] for the general framework.

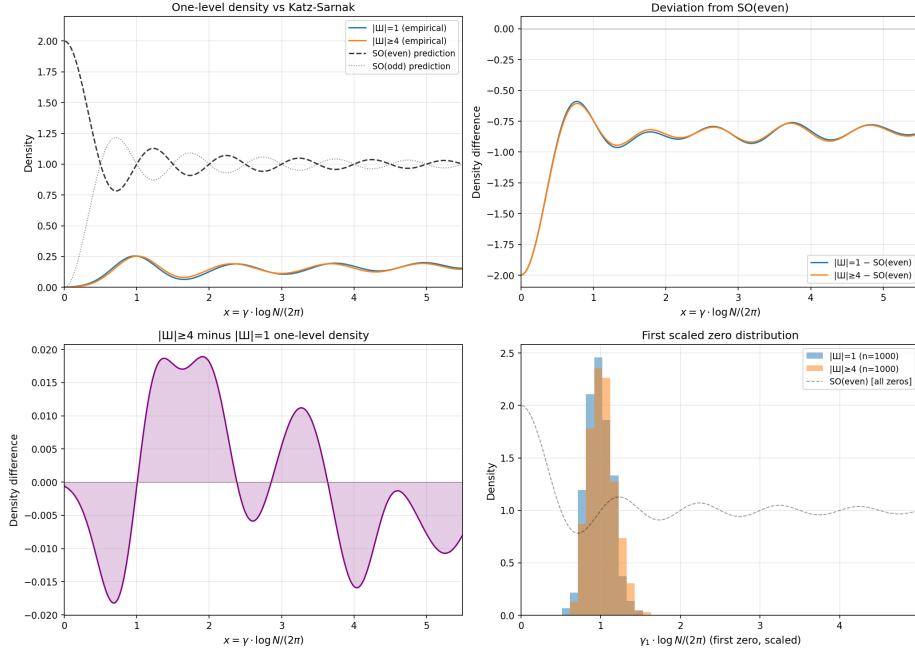


Figure 10. One-level density compared with Katz–Sarnak predictions. Top left: empirical densities for both III groups versus SO(even) and SO(odd). Top right: deviation from SO(even). Bottom left: difference between the two III groups. Bottom right: first scaled zero histograms.

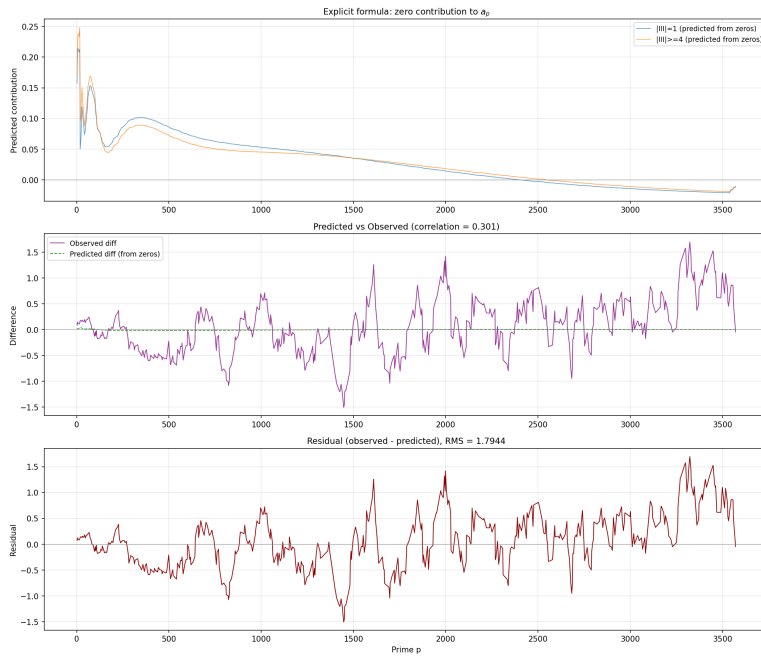


Figure 11. Explicit formula prediction. Top: predicted a_p contribution from first five zeros. Middle: predicted vs. observed difference in murmuration profiles (correlation $r = 0.30$). Bottom: residual.

9. FUTURE DIRECTIONS

- (1) **Full Sawin–Sutherland prediction.** Computing the complete murmuration density (including Bessel function sums and the full local factor structure) for each Tamagawa stratum would provide a quantitative test of the local factor mechanism.
- (2) **Ratios conjecture for the III modulation.** Cowan’s ratios conjecture approach to murmurations [1] could potentially be conditioned on $|\text{III}|$ to predict the observed crossover shape.
- (3) **More zeros.** Our explicit formula analysis uses only 5 zeros per curve (correlation 0.30). Computing 50–100 zeros would test whether the full zero spectrum accounts for the entire III effect quantitatively.
- (4) **Larger conductor ranges.** Our Frobenius trace data extends to conductor 100,000. Testing at conductor 500,000+ would probe whether the III effect is asymptotic.
- (5) **Rank-1 curves.** A preliminary analysis with 2,371 rank-1 curves having $|\text{III}| \geq 4$ in our dataset yields an RMS difference of 0.97 ($p = 0.001$ by permutation test), suggesting the III modulation extends to rank 1. Confirmation with larger datasets at higher conductor would be valuable.
- (6) **p -adic structure of the III effect.** Decomposing curves by the p -part of III reveals that the 2-primary ($|\text{III}| = 4$) and 3-primary ($|\text{III}| = 9$) modulations have qualitatively different shapes (correlation -0.10 between their deviations from $|\text{III}| = 1$). This suggests the murmuration modulation is sensitive to the p -adic structure of III, not just its order, and may connect to Iwasawa theory.
- (7) **Random matrix refinements.** Our comparison with Katz–Sarnak (Section 8.3) confirms that both III groups share $\text{SO}(\text{even})$ symmetry, with the displacement concentrated in the first zero. A natural next step is to derive the expected γ_1 shift from random matrix theory, given the constraint that the characteristic polynomial takes a fixed value at a specific point (the analogue of fixing $L(E, 1)$).

ACKNOWLEDGMENTS

Computations were performed using SageMath [7] and the Cremona database [2]. The author thanks Yang-Hui He, Kyu-Hwan Lee, Thomas Oliver, and Alexey Pozdnyakov for inspiration behind this research [4], and the developers of the LMFDB [5] for making elliptic curve data widely accessible for researchers.

REFERENCES

- [1] A. Cowan, *Murmurations and the ratios conjecture*, preprint, 2024, [arXiv:2408.12723](https://arxiv.org/abs/2408.12723).
- [2] J. E. Cremona, *Algorithms for Modular Elliptic Curves*, 2nd ed., Cambridge University Press, 1997. Database available at <https://johncremona.github.io/ecdata/>.
- [3] B. H. Gross and D. B. Zagier, *Heegner points and derivatives of L -series*, *Inventiones Mathematicae* **84** (1986), 225–320.
- [4] Y.-H. He, K.-H. Lee, T. Oliver, and A. Pozdnyakov, *Murmurations of elliptic curves*, *Experimental Mathematics* **33** (2024), no. 4, 604–613, [arXiv:2204.10140](https://arxiv.org/abs/2204.10140).
- [5] The LMFDB Collaboration, *The L -functions and Modular Forms DataBase*, <https://www.lmfdb.org>, 2024.
- [6] A. Alessandretti, J. Cremona, and L. Sheridan, *ML approaches to the Shafarevich–Tate group of elliptic curves*, preprint, 2024, [arXiv:2412.18576](https://arxiv.org/abs/2412.18576).
- [7] The Sage Developers, *SageMath, the Sage Mathematics Software System (Version 10.8)*, <https://www.sagemath.org>, 2025.
- [8] W. Sawin and A. V. Sutherland, *Murmurations for elliptic curves ordered by height*, preprint, 2025, [arXiv:2504.12295](https://arxiv.org/abs/2504.12295).
- [9] H. Iwaniec and E. Kowalski, *Analytic Number Theory*, AMS Colloquium Publications, vol. 53, American Mathematical Society, 2004.
- [10] V. A. Kolyvagin, *Finiteness of $E(\mathbb{Q})$ and $\text{III}(E, \mathbb{Q})$ for a subclass of Weil curves*, *Izvestiya Akademii Nauk SSSR Seriya Matematicheskaya* **52** (1988), no. 3, 522–540.
- [11] N. Zubrilina, *Murmurations*, *Inventiones mathematicae* **241** (2025), 627–680, [arXiv:2310.07681](https://arxiv.org/abs/2310.07681).

THE UNIVERSITY OF ARIZONA, TUCSON, AZ
 Email address: wachs@arizona.edu